Anal Bioanal Chem (2010) 398:1927–1936
DOI 10.1007/s00216-010-4099-4

ORIGINAL PAPER

Total internal reflection ellipsometry as a label-free assessment method for optimization of the reactive surface of bioassay devices based on a functionalized cycloolefin polymer

Nam Cao Hoai Le · Vladimir Gubala · Ram P. Gandhiraman · Conor Coyle · Stephen Daniels · David E. Williams

Received: 30 April 2010 / Revised: 3 August 2010 / Accepted: 4 August 2010 / Published online: 29 August 2010

Abstract We report a label-free optical detection technique, called total internal reflection ellipsometry (TIRE), which can be applied to study the interactions between biomolecules and a functionalized polymer surface. Zeonor (ZR), a cycloolefin polymer with low autofluorescence, high optical transmittance and excellent chemical resistance, is a highly suitable material for optical biosensor platforms owing to the ease of fabrication. It can also be modified with a range of reactive chemical groups for surface functionalization. We demonstrate the applications of TIRE in monitoring DNA hybridization assays and human chorionic gonadotrophin sandwich immunoassays on the ZR surface functionalized with carboxyl groups. The Ψ and Δ spectra obtained after the binding of each layer of analyte have been fitted to a four-layer ellipsometric model to quantitatively determine the amount of analytes bound specifically to the functionalized ZR surface. Our proposed TIRE technique with its very low analyte consumption and its microfluidic array format could be a useful tool for evaluating several crucial parameters in immunoassays, DNA interactions, adsorption of biomolecules to solid surfaces, or assessment of the reactivity of a functionalized polymer surface towards a specific analyte.

Keywords Total internal reflection ellipsometry · Cycloolefin polymer · Plasma-enhanced chemical vapour deposition · Immunoassays · DNA hybridization · Microfluidics

Published in the special issue Optical Biochemical and Chemical Sensors (Europtrode X) with guest editor Jiri Homola.

N. C. H. Le (✉) · V. Gubala · R. P. Gandhiraman · C. Coyle · S. Daniels · D. E. Williams
Biomedical Diagnostics Institute (BDI), Dublin City University, Dublin 9, Republic of Ireland
e-mail: nam.caohoaile@dcu.ie

C. Coyle · S. Daniels
National Centre for Plasma Science and Technology (NCPST), Dublin City University, Dublin 9, Republic of Ireland

D. E. Williams
MacDiarmid Institute for Advanced Materials and Nanotechnology, Department of Chemistry, University of Auckland, Auckland 1142, New Zealand

Introduction

Zeonor (ZR), a type of cycloolefin polymer (COP), with excellent optical and chemical properties and good machinability, has received increasing attention from the biomedical diagnostics industry for the development of low-cost, disposable biosensor platforms, appropriate for point-of-care applications [1, 2]. Pristine ZR substrates are chemically inert and therefore need to be modified to have suitable physicochemical properties for biosensor applications. Surface functionalization of ZR to introduce chemical functional groups for immobilization of proteins or oligonucleotides is a critical step towards the realization of low-cost biosensors.

Several techniques have been proposed to functionalize ZR with carboxylic or amine functional groups using both standard liquid phase chemistry as well as plasma-enhanced chemical vapour deposition (PECVD) [3–9]. The quality of the functional films produced on the ZR surface has a significant influence on the performance of the biosensor devices. In the above-mentioned work, fluorescence detec-

tion was used as the principal method to evaluate the reactivity of the functional films to target biomolecules. Quantitative data about the number of bound molecules from these experiments are usually deduced from fluorescence intensity data. However, the attachment of the fluorophores to a biomolecule is a time- and material-consuming process, which can frustrate the need to perform rapid and efficient assessments of the quality of the surface with respect to its use with specific reagents. Accordingly, for this purpose, a label-free detection method could be an advantageous alternative to fluorescence detection methods [10]. Surface plasmon resonance has been widely applied as a label-free detection technique to study the interactions of molecules with functionalized gold surfaces [11, 12] as well as with polymer surfaces [13–15]. Recently, total internal reflection ellipsometry (TIRE) or surface plasmon enhanced ellipsometry (SPEE) has been proposed as an alternative label-free method to detect the binding of various analytes to a metal surface, typically gold [16–24]. Here, we propose applying TIRE to monitor the binding of the biomolecules to a ZR surface functionalized with film containing carboxyl groups. A specialized poly (methyl methacrylate) (PMMA) microfluidic flow-cell has been developed, allowing us to significantly reduce the volumes of analytes and the amount of gold-based sensing substrates used in the experiments. The objective of this study was to develop an efficient method for assessing both surface activation treatments and new bioreagents applied to these surfaces, in a format where the surfaces reasonably resemble those that will be found in a final mass-produced device. The design was specifically directed towards the assessment of single-chain antibodies prepared by phage display. To this end, we have successfully demonstrated the applications of TIRE in detection of two kinds of bioassays on the carboxyl-functionalized ZR surface: DNA hybridization assay and human chorionic gonadotrophin (hCG) sandwich immunoassays. Together with fitting of the measured Ψ and Δ data, this method allows us to quantitatively estimate the surface excess of biomolecules bound to the functionalized ZR surface. This method also provides information about the stability of functionalized polymer surfaces upon contact with aqueous solutions as well as the reactivity of those surfaces towards a specific analyte, both of which are important to improve the performance of ZR-based biosensor devices.

Experimental

Materials

COP slides (Zeonor® 1060R) (ZR) (25 mm×75 mm, 1 mm thick) were supplied by Åmic (Uppsala, Sweden). Gold-coated standard glass slides (Ti/Au 2 nm/48 nm, 26 mm×76 mm, 1 mm thick) were purchased from Phasis Sarl (Geneva, Switzerland). *N*-(3-Dimethylaminopropyl)-*N*′-ethylcarbondiimide hydrochloride (EDC), *N*-hydroxysuccinimide (NHS) and xylene were purchased from Sigma-Aldrich (Dublin, Ireland). All chemicals were used as received without further purification. Amino-modified single-stranded DNAs (ssDNAs) (5′-ACG-GCA-GTG-TTT-AGC-3′) (*Sa19* ssDNA, 15-mer), complementary ssDNAs (5′-GCT-AAA-CAC-TGC-CGT-3′) (*Sa19 rev comp* ssDNA, 15-mer) and non-complementary ssDNAs (5′-AAG-TTT-CTT-CTA-AAC-AGA CT-3′) (*Sa20 non-comp* ssDNA, 20-mer) were purchased from Eurofins MWG Operon (Ebersberg, Germany). The antibodies and antigen used in this work were anti-α-human chorionic gonadotropin (anti-α-hCG) (clone 3299:4), anti-β-hCG (clone 3468:2) and hCG (B250K/620; 250,000 mIU/ml) kindly donated by Inverness Medical Innovations (Bedford, UK).

Preparation of sensing substrate

A scheme for the preparation of the sensing substrate is illustrated in Fig. 1. A COP slide was cut into small pieces and dissolved in xylene at 0.25 wt%w/v to make the raw ZR solution. The ZR solution was then filtered through a poly(tetrafluoroethylene) (PTFE) filter (pore size 0.2 μm) (Chromafil Xtra PTFE-20/25 Macherey-Nagel, Duren, Germany) to eliminate the precipitates and dust particles. The ZR solution was then spin-coated onto a gold-coated glass slide at 1,300 rpm in 30 s with acceleration in 2 s and 2,000 rpm in 5 s with acceleration in 2 s. The solvent xylene was naturally evaporated, leaving a thin ZR film [25]. The substrate was subsequently treated in an oxygen

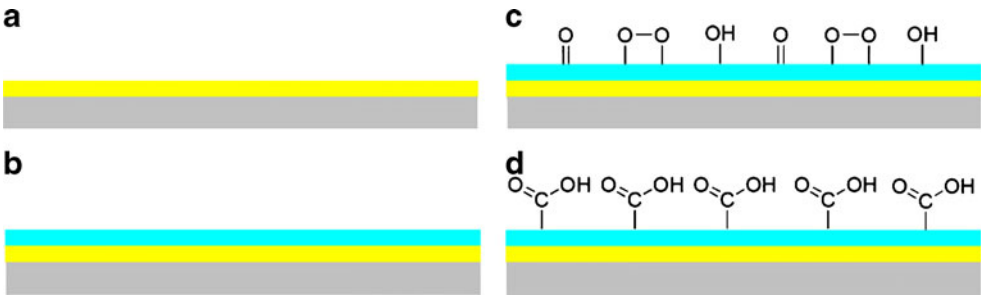

Fig. 1 Preparation of the sensing substrate containing carboxyl functional groups: **a** gold-coated glass slide, **b** Zeonor (ZR) spin-coating, **c** oxygen plasma treatment, **d** COOH film deposition (only the top layer of the film is illustrated)

plasma for 1 min and then the carboxylic acid functionalized coatings were prepared by sequential deposition of tetraethylorthosilicate (TEOS) and acrylic acid by low-temperature PECVD [7–9]. The resulting substrates exhibited increased COOH functionality for protein adhesion, an improved signal-to-noise ratio and a high resistance to washing. Given the nature of the technique, the details of the reaction mechanism are unclear. However, we hypothesize that the TEOS molecules initially form a thin bonding layer on COP, onto which acrylic acid is further polymerized. The polymerization process is initialized and assisted by plasma and results in a fabrication of a relatively homogeneous layer with high density of carboxylic acids. The very low water contact angle of the film also suggests that TEOS might be inserted into the sensing COOH layer, cross-linking the polymerized acrylic acid molecules and forming an abundance of silanols and silyl ethers [unpublished data].

At different stages of the preparation of the sensing substrates, the wettability and the thickness of the deposited films were analysed. The film wettability was analysed by measuring the water contact angle using the First Ten Angstroms (Portsmouth, VA, USA) FTA200 contact-angle analyser. High-purity high performance liquid chromatography grade water (Sigma-Aldrich, Dublin, Ireland) was used for the measurements. Images of drops were recorded with a CCD camera and analysed using the accompanying software. The thicknesses of the films deposited on the gold sensing substrate were measured by a UVISEL spectroscopic ellipsometer (HORIBA Jobin Yvon, France) in external mode. A three-layer model (BK7 glass, gold and organic layer) was used in the fitting with DeltaPsi 2 software (HORIBA Jobin Yvon, France) to obtain the thickness of the gold, ZR and COOH films from the measured Ψ and Δ spectra. The refractive indices of BK7, gold and the organic layer are detailed in "Fitting data and calculate surface excess".

Microfluidic flow-cell fabrication

The microfluidic flow-cell, containing four layers, was fabricated in PMMA and pressure-sensitive adhesive (PSA) using a CO_2 ablation laser machining system (Fig. 2). The top PSA layer, 50-μm thickness, contains five reaction microwells glued with the sensing substrate on top and a PMMA (250-μm thickness) connecting hole layer at the bottom. Inlets and outlets were also defined on this PMMA layer. Next is a PSA channel layer, also 50 μm thick, containing five sets of channels (500-μm width) to connect the inlets and outlets to the reaction microwells through the PMMA connecting hole layer. Underneath is a base PMMA layer (250-μm thickness) to seal the PSA channel layer above. Punched slabs of poly(dimethylsiloxane) (PDMS) (4 mm×4 mm×3 mm) as connectors were glued at

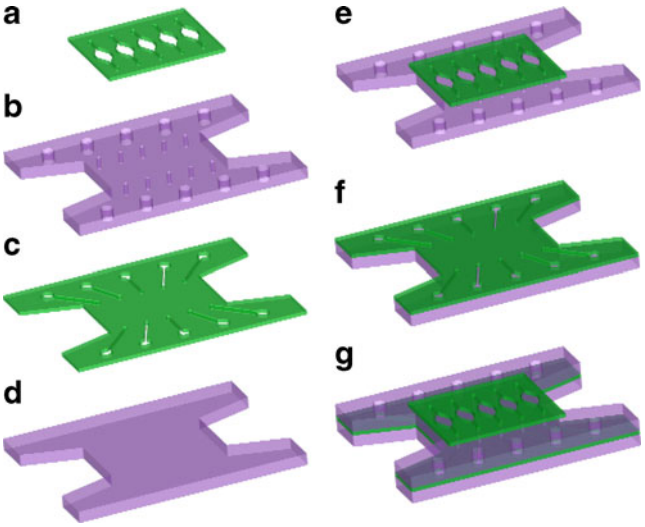

Fig. 2 Fabrication process of microfluidic flow-cell in poly(methyl methacrylate) (PMMA) and pressure-sensitive adhesive (PSA): **a** top PSA layer containing five reaction microwells (the volume of each microwell is 4.7 μl), **b** connecting hole PMMA layer, **c** PSA channel layer, **d** bottom PMMA layer, **e** bonding of top PSA layer and connecting hole PMMA layer, **f** bonding of PSA channel layer and bottom PMMA layer, **g** complete four-layer microfluidic flow-cell

the outlets of the top PMMA layer using PSA. With this design, we were able to incorporate five reaction microwells onto a sensing substrate which is half of a gold-coated standard glass slide (26 mm×76 mm). Furthermore, the volume of the microwells was substantially reduced to approximately 4.7 μl compared with a typical few millilitres in previous works [16–22]. This feature is very important for experiments requiring expensive analytes such as proteins or oligonucleotides.

TIRE experimental setup

TIRE or SPEE is a spectroscopic ellipsometry measurement method operated under the total internal reflection condition [16–24]. As in a conventional spectroscopic ellipsometry method, TIRE also measure two ellipsometric angles, Ψ and Δ, versus wavelengths. These Ψ and Δ values are defined by the ratio ρ of the reflection coefficients R_p and R_s for components of light polarized parallel and perpendicular, respectively, to the plane of incidence following the ellipsometry equation [26]:

$$\rho = \frac{R_p}{R_s} = \tan \Psi \exp(i\Delta). \quad (1)$$

It is obvious that Ψ and Δ also depend on angle of incidence Φ and wavelengths λ. The refractive indices and thicknesses of each layer of the reflecting surfaces can be found by fitting the measured Ψ and Δ data to a defined model.

Our TIRE experimental setup was based on a UVISEL spectroscopic ellipsometer (HORIBA Jobin Yvon, France) (Fig. 3a). The sensing substrate was first glued to the fabricated microfluidic flow-cell by adhesion of the PSA reaction microwell layer. A BK7 prism was placed on top of the sensing substrate with an intermediate refractive index matching oil and secured by tapes (Fig. 3b). A syringe pump (Harvard Apparatus, Boston, USA) was connected to the outlet of one microwell of the flow-cell through polymer tubing and a PDMS connector. A droplet of analyte (20–30 μl) injected at the corresponding inlet was sucked into the microwell by the syringe pump operating in the withdraw mode [27]. The flow rate was controlled to within 4–5 μl/min. The volume of analyte is always larger than the volume of the microwell (4.7 μl) to make sure the microwell is always filled with analyte and is not dried during measurements. TIRE measurements were conducted at an external angle of incidence of 70° with wavelengths ranging from 400 nm to 850 nm. After refracting at the air/BK7 prism interface, the light rays enter the interface of the sensing substrate and the aqueous buffer at an angle of incidence ranging from 68.263° to 68.308° (for wavelengths from 400 to 850 nm) owing to the dispersion at the air/BK7 interface. If the wavelength range is broader, the variation in the incident angles is larger and could cause some distortion in the detected signals since the detector will received the reflected light beams at different reflecting angles. However, with this current wavelength range, the variation in incident angles is negligible and we have not detected any distortion in our measured Ψ and Δ signals. The integration time was 200 ms and the spectral resolution varied from 2 to 10 nm. Although the flow-cell contains five microwells, only one assay was performed at a time on one microwell to prevent any possible shifting of the light rays in the optical setup. In all experiments, the Ψ and Δ spectra were always recorded after the syringe pump had been turned off and the measuring microwell had been filled with phosphate-buffered saline (PBS; pH 7.4). DeltaPsi 2 software (HORIBA Jobin Yvon, France) was used for fitting the data from the measured Ψ and Δ spectra from TIRE. Details of the fitting procedure are summarized in "Fitting data and calculate surface excess".

TIRE experimental procedure

First, we tested the stability of the COOH film on the sensing substrate inside one of the microwells by replacing new PBS every 60 min in a 120-min period during which three sets of Ψ and Δ were recorded separated by 60 min. Three sets of Ψ and Δ spectra were superimposed on the same plot to check if they still remained overlapped.

The DNA hybridization assay was conducted in a fresh microwell after the baseline Ψ and Δ spectra of the COOH surface in PBS had been recorded. Thirty microlitres of 10^{-5} M aminated *Sa19* ssDNA in 100 mM EDC in 2-(*N*-morpholino)ethanesulfonic acid (MES; pH 8.0) buffer was then pumped into the microwell and allowed to react for 60 min (Fig. 4, steps b, c). A second set of Ψ and Δ spectra, which correspond to the registration of the binding of the capture *Sa19* ssDNA, were measured after the microwell had been rinsed with 50 μl PBS. Next, 30 μl of 10^{-5} M complementary *Sa19 rev comp* ssDNA in hybridization buffer (150 mM NaCl, 150 mM saline/sodium citrate buffer, pH 7.0) was pumped into the microwell and also allowed to react for 60 min before rinsing the microwell with 50 μl PBS. A third set of Ψ and Δ spectra were then recorded, corresponding to the registration of the complementary *Sa19 rev comp* ssDNA to the capture *Sa19* ssDNA. We also conducted two negative control experiments in two different microwells. The first negative control experiment was conducted with mismatched *Sa20 non-comp* ssDNA at concentration of 10^{-5} M in the same hybridization buffer to confirm the specificity of the captured ssDNA probes. The second negative control experiment was performed to assess the COOH surface capture efficiency of the aminated *Sa19* ssDNA without EDC in the MES buffer.

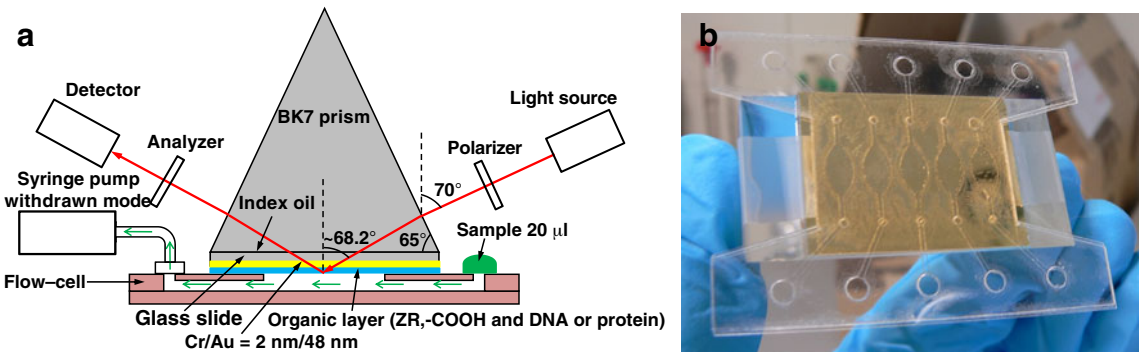

Fig. 3 **a** Total internal reflection ellipsometry experimental setup (not to scale) fitted on a UVISEL spectroscopic ellipsometer and a Harvard Apparatus syringe pump. **b** Assembly of the prism, the sensing substrate and the five-microwell flow-cell

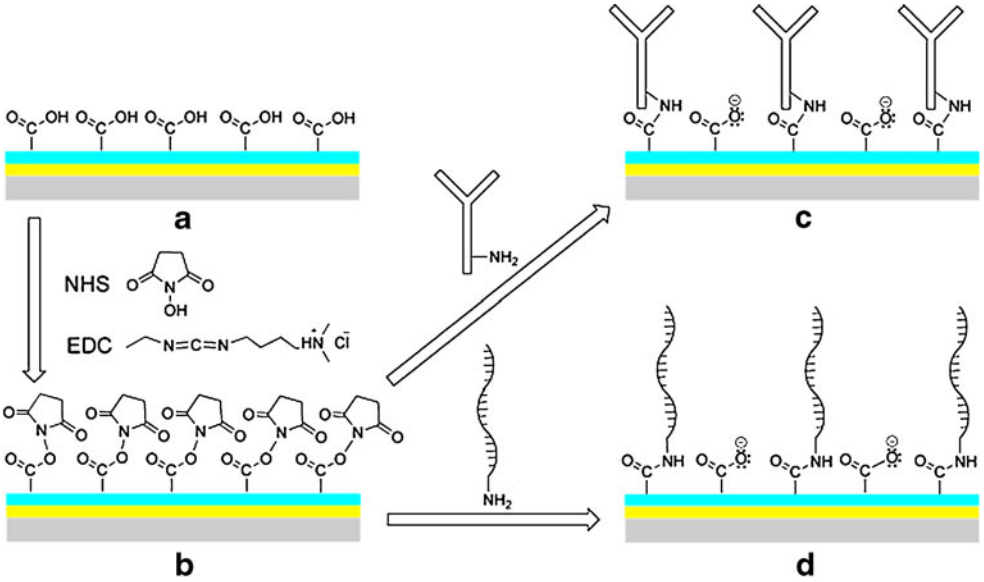

Fig. 4 Activation of the COOH surface (only the top layer of the film is illustrated) by EDC (for single-stranded DNA, ssDNA) or EDC/NHS (for antibody) (*a*, *b*) and binding to the activated COOH surface by antibody anti-α-human chorionic gonadotrophin (anti-α-hCG) (*c*) or by aminated *Sa19* ssDNA (*d*)

For hCG sandwich immunoassays, the baseline Ψ and Δ spectra of the COOH surface in PBS were also recorded first. The reaction microwell was then activated by 100 mM EDC and 100 mM NHS in deionized water for 15 min and then rinsed with 50 μl PBS. Thirty microlitres of capture anti-α-hCG antibody in PBS (pH 7.4) at a concentration of 2, 20 or 200 μg/ml was pumped into the microwell and allowed to react for 30 min before rinsing the microwell with 50 μl PBS (Fig. 4, steps b–d). Ψ and Δ spectra of bound anti-α-hCG on the COOH surface were then measured. Thirty microlitres of hCG solution in PBS at a fixed concentration of 2 μg/ml was then injected and also allowed to react with the surface-bound anti-α-hCG for 30 min. A third set of Ψ and Δ spectra were recorded after the microwell had been rinsed with 50 μl PBS. Finally, a 30-μl solution of anti-β-hCG in PBS at the same concentration as that of the capture anti-α-hCG was pumped in, allowed to react for 30 min and the microwell was rinsed with 50 μl PBS before the fourth set of Ψ and Δ spectra were measured.

Fitting data and calculate surface excess

The four-layer ellipsometric model summarized in Table 1 was used in the fitting of the measured Ψ and Δ spectra by using DeltaPsi 2 software (HORIBA Jobin Yvon, France) to deduce the thickness of each organic layer added to the gold surface [19–22]. The refractive indices of all four layers in the model were fixed in the fitting. The thickness of gold was obtained from previous external spectroscopic ellipsometry measurements and was fixed in the fitting. The only variable is the thickness of the organic layer including the ZR film, the COOH film and the DNA or the protein layer. The refractive index of the BK7 prism was obtained from the SCHOTT BK7 data sheet. The refractive indices of gold and water were obtained from the software library based on Palik [28, 29]. The refractive indices of the ZR film, the COOH film and the DNA or the protein film are assumed to follow the same Cauchy dispersion formula obtained from [20]. This assumption inevitably compromised the determination of the exact refractive index of each organic material layer but it helped to uncouple the refractive indices and film thicknesses in ellipsometric fitting [19–22, 30].

The thicknesses of the ZR film and the COOH had been found previously by measurement and fitting in the external mode (see "Preparation of sensing substrate"). The thickness of the plasma-treated ZR film (before COOH film deposition by PECVD) was found to be 4.9 nm. The thickness of the COOH film was 4.7 or 6.7 nm for the

Table 1 Four-layer model used in the fitting of the measured Ψ and Δ spectra

Layer	Materials	Thickness	Refractive index (all fixed)
1	BK7	∞	SCHOTT BK7 data sheet
2	Au	52 nm (fixed)	From Palik [28]
3	Organic layer (Zeonor, COOH, DNA or protein)	Variable	Cauchy: $A + B/\lambda^2 + C/\lambda^4$ *[20]* A=1.415, B=0.01 nm^2, C=0
4	Water	∞	From Palik [29]

sample used in DNA hybridization assays and hCG immunoassays, respectively. The total thickness of the ZR film and the COOH film was used as a lower limit to guide the software to find the thickness change during the fitting. Accordingly, the total organic layer thickness is increased when a subsequent biolayer, either the DNA or the protein film, is built on to the COOH surface.

For DNA hybridization assays, we could only deduce the effective thickness changes after the immobilization of the capture ssDNA and then the hybridization of the complementary ssDNA as mentioned in "DNA hybridization assays". However, for the hCG immunoassays, the availability of the change in the refractive index of the protein solution with increasing concentration enabled us to employ De Feitjer's formula to determine the amount of bound proteins from their thicknesses [31]:

$$\Gamma = \frac{\tau(n - n_{\mathrm{w}})}{10 \times \mathrm{d}n/\mathrm{d}c}, \qquad (2)$$

where Γ (mg/m^2) is the protein surface excess, τ is the thickness of the proteins (nm), n_{w} is the refractive index of the aqueous phase at 633 nm, n is the refractive index of the protein at 633 nm (Table 1) and dn/dc is the change in the refractive index of the protein solution with increasing concentration, which is close to 0.18 cm^3/g for a variety of proteins [31].

Results and discussion

Water contact angle, film thicknesses and stability of sensing substrate

The water contact angle changes after the deposition of ZR and after the introduction of COOH groups on the gold-coated glass slide are plotted in Fig. 5a. The deposition of ZR caused a small increase in water contact angle due to the hydrophobic nature of ZR. However, after the deposition of COOH film, the water contact angle dropped substantially to approximately 23°. This change in contact angle is attributed to the hydrophilic characteristic of the COOH functional groups. Spectroscopic ellipsometric measurements were performed to confirm the successful deposition of ZR and COOH on gold-coated glass substrates (Fig 5b). After ZR deposition, the original Δ spectrum shifted downwards from "gold" to "ZR/gold". The ellipsometric fitting confirmed that a ZR layer of 9.8 nm was successfully deposited on the gold slide. However, the thickness of the ZR layer was reduced to 4.9 nm (not shown) after being treated in oxygen plasma for 1 min at 60 W before the deposition of COOH film [25]. Next, the downward shift of the Δ spectrum from "ZR/gold" to "COOH/ZR/gold" corresponded to an increase in thickness of 4.7 nm, which was caused by the deposition of the functional COOH film onto the ZR-coated gold-coated glass surface. These water contact angle and spectrocopic ellipsometry measurements confirmed the presence of ZR and COOH films on the sensing substrate. The superimposition of three sets of Ψ and Δ spectra of COOH film on the sensing substrate measured in TIRE mode over 120 min showed that no shifts of any spectra were detected (Fig. 6). Since there was no change in refractive index within the solid/liquid interface, the overlap of the spectra confirmed the stability of the thickness of the COOH film upon contact with aqueous PBS.

DNA hybridization assays

Ψ and Δ spectra of the complete DNA hybridization assay are plotted in Fig. 7a and b, respectively. The introduction of the capture aminated *Sa19* ssDNA (15-mer) solution and then the complementary *Sa19 rev comp* ssDNA (15-mer) solution resulted in large shifts in both Ψ and Δ spectra from the initial Ψ and Δ spectra of the COOH surface when the microwell was filled with PBS. In the first negative control experiment, a mismatched *Sa20 non-*

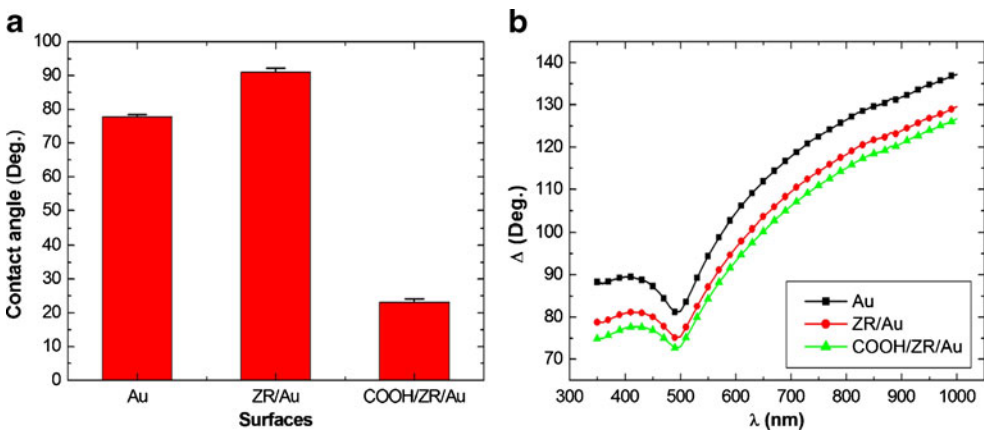

Fig. 5 **a** Surface contact angle changes on a gold-coated glass slide after spin-coating ZR and then introducing COOH functional film. **b** Corresponding Δ spectra shift after ZR spin-coating (before plasma treatment) and COOH film deposition

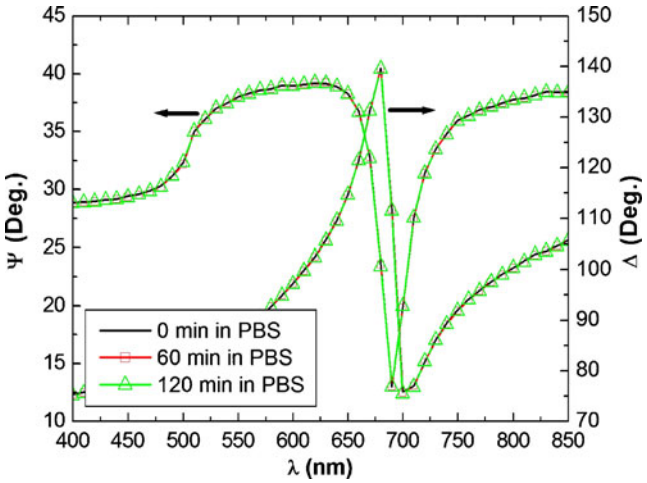

Fig. 6 Superimposition of three sets of Ψ and Δ spectra of COOH film on the sensing substrate in contact with phosphate-buffered saline (*PBS*; pH 7.4) measured over a period of 120 min separated by 60 min

comp ssDNA solution (20-mer) was incubated for 60 min after the capture *Sa19* ssDNA had been immobilized to assess the non-specific hybridization and non-specific binding effect. As seen in Fig. 7c and d, the introduction of the non-complementary ssDNA solution did not result in any shifts in the Ψ and Δ spectra. Therefore, the effects of non-specific binding and non-specific hybridization were minimal. The second negative control experiment, conducted by incubating the aminated *Sa19* ssDNA solution without the activating agent EDC, showed that only a very small shift in Ψ and Δ spectra was observed after 60 min (Fig. 7e, f). A four-layer ellipsometric model as presented in Table 1 was used for fitting the measured Ψ and Δ spectra to deduce the effective thickness of each DNA layer. It was found that only a small amount of aminated *Sa19* ssDNA, 0.25±0.12 nm in thickness, was captured on the COOH surface for the second negative control experiment. For the positive experiment, fitting of Ψ and Δ spectra also gave effective thicknesses of both the capture ssDNA and the hybridized DNA of 2.02± 0.16 nm and 3.49±0.42 nm, respectively. It is interesting to note that the hybridization resulted in an increase in effective thickness. This suggests that the capture ssDNA could form a layer composed of coiled oligonucleotides, which are stretched out during the hybridization to its complementary strand. This observation is in good agreement with results previously reported in the literature [32, 33].

hCG sandwich immunoassays

Similarly to the DNA hybridization assays, the hCG sandwich immunoassays were successfully realized after activating the COOH surface with an EDC/NHS mixture inside the TIRE microwells. The covalent binding of the capture anti-α-hCG antibody caused a large and distinct shift in both Ψ and Δ spectra. These shifts increased with increasing concentration of anti-α-hCG, in the range from 2 to 200 μg/ml (Fig. 8). It is noticeable to see that the original plasmon resonance wavelength for these assays (i.e. 727.5 nm) was different from that in the DNA hybridization assay described earlier (i.e. 690 nm). This discrepancy could be due to the difference in COOH film thickness deposited in each batch when the sensing substrates were prepared. The COOH thickness in the case of the DNA hybridization assay was approximately 4.7 nm, whereas that for the hCG assay was approximately 6.7 nm. The subsequent binding of the hCG antigen at 2 μg/ml to the capture anti-α-hCG caused another shift in both Ψ and Δ spectra (Fig. 8). Finally, the binding of the second antibody anti-β-hCG caused a third shift in both Ψ and Δ spectra (Fig. 8). Compared with the first shift after binding of anti-α-hCG, the second and the final shifts in the Ψ and Δ spectra for binding of hCG and anti-β-hCG, respectively, were small and not so distinctive. We reason that, similarly to the case of adsorption of anti-β-hCG to a silica surface, here the first anti-α-hCG antibodies could predominantly bind to COOH film with the same lying-down or "flat-on" orientation and they were arranged like a disordered stack of dish plates [34]. The antigen hCG then filled in some of the gaps and contributed some more dish plates lying in and on the first layer of anti-α-hCG antibodies. Similarly, the second anti-β-hCG antibody filled in more of the remaining gaps. Hence, the apparent thickness change was small, corresponding to the small shifts in the Ψ and Δ spectra after the binding of hCG and anti-β-hCG. Similar reasoning concerning the changes in molecular conformation on the surface could also explain why, for the case of the DNA hybridization assay, the shifts in Ψ and Δ spectra after binding of the complementary ssDNA were still relatively large compared with those of the capture ssDNA (Fig. 7a, b). These large shifts could be due to the possibility that the DNA strands were stretched out upon hybridization unlike the "fill-in" fashion upon binding of antigen and antibody. However, there should be further investigations using a complementary technique such as atomic force microscopy or neutron reflectivity to study the actual orientation of the proteins when forming complex sandwich immunoassays at the functionalized ZR surface [34]. Several optical detection methods have been proposed to detect hCG in sandwich immunoassays with very high sensitivity [35–38]. The concentration of hCG in the current work was still relatively high: however ,it has been shown that TIRE can successfully be applied to detect hCG capture and labelling in sandwich immunoassays. For further improvements in the sensitivity, the optimal thickness of the gold film, the COOH film uniformity and

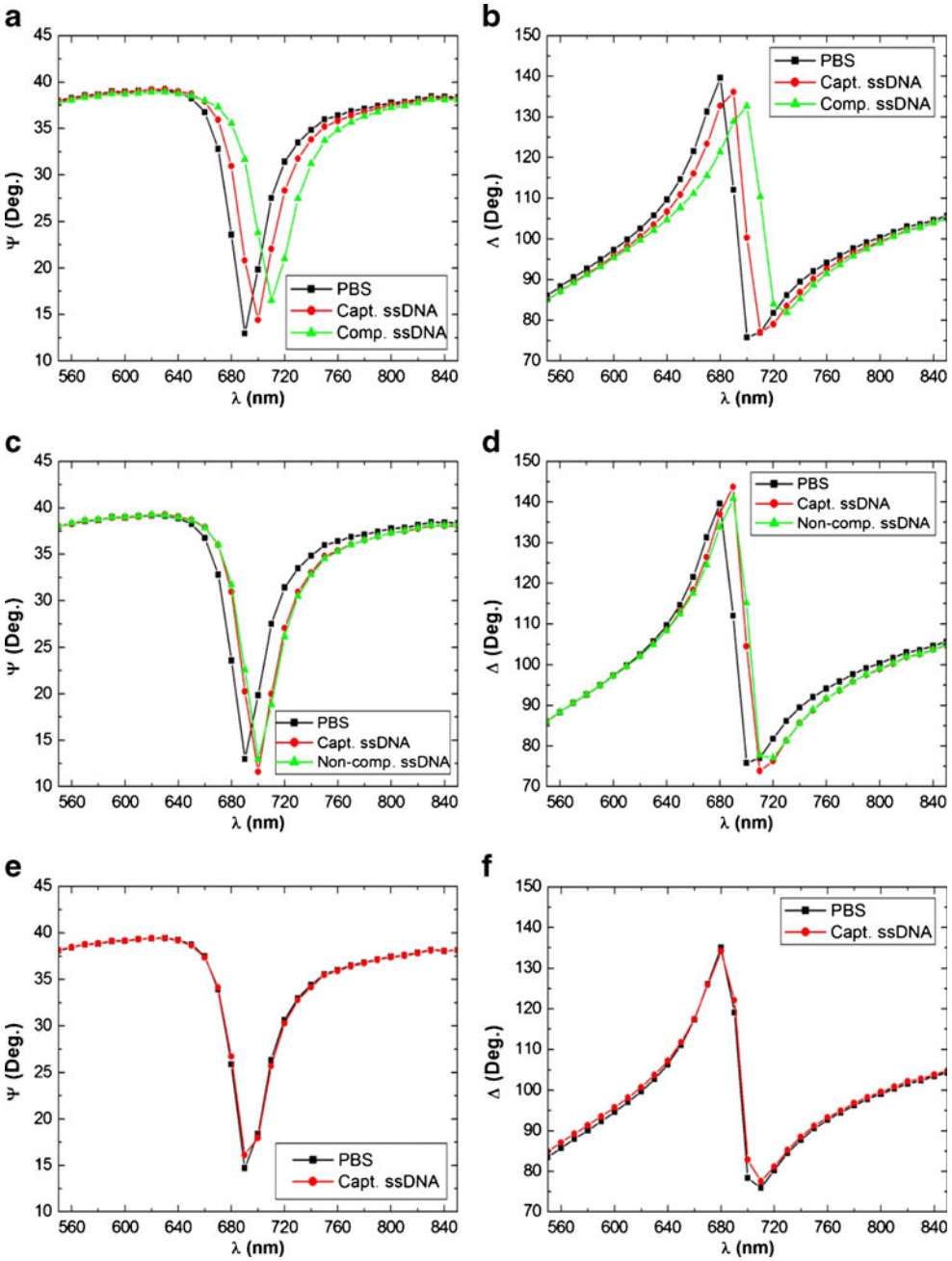

Fig. 7 **a**, **b** Ψ and Δ spectral shifts after binding of the capture of aminated *Sa19* ssDNA (15-mer) at 10^{-5} M and hybridized with complementary *Sa19 rev comp* ssDNA (15-mer) at 10^{-5} M. **c**, **d** Ψ and Δ spectral shifts were only observed for binding of the capture *Sa19* ssDNA (15-mer) at 10^{-5} M but not for the mismatched *Sa20 non-comp* ssDNA (20-mer) at 10^{-5} M. **e**, **f** Capture of aminated *Sa19* ssDNA (15-mer) at 10^{-5} M without EDC activation; Ψ and Δ spectral shifts were minimal

non-specific binding of the analyte to the PMMA flow-cell surface need to be addressed.

The results of the fitting and the calculation of the protein surface excesses for three hCG immunoassays are summarized in Table 2. As expected, the surface excesses of the anti-α-hCG antibodies increased with increasing concentrations of the capture anti-α-hCG in the initial surface functionalization. Similarly, surface excesses of the antigen hCG also increased with increasing surface excess of anti-α-hCG. However, this trend was somewhat discontinued for the second antibody, anti-β-hCG. The surface excesses of anti-β-hCG do not follow any particular trend. There should be further investigations to understand the effects of the surface excesses of the first capture antibody and antigen on the surface excesses of the second antibody [30].

Conclusions

A label-free, low volume and in situ TIRE detection technique to monitor the binding of biomolecules to a functionalized ZR surface in a microfluidic array format has been proposed. The design of a specialized PMMA flow-cell enabled us to fit five reaction microwells onto the sensing substrate, half of a gold-coated standard glass slide.

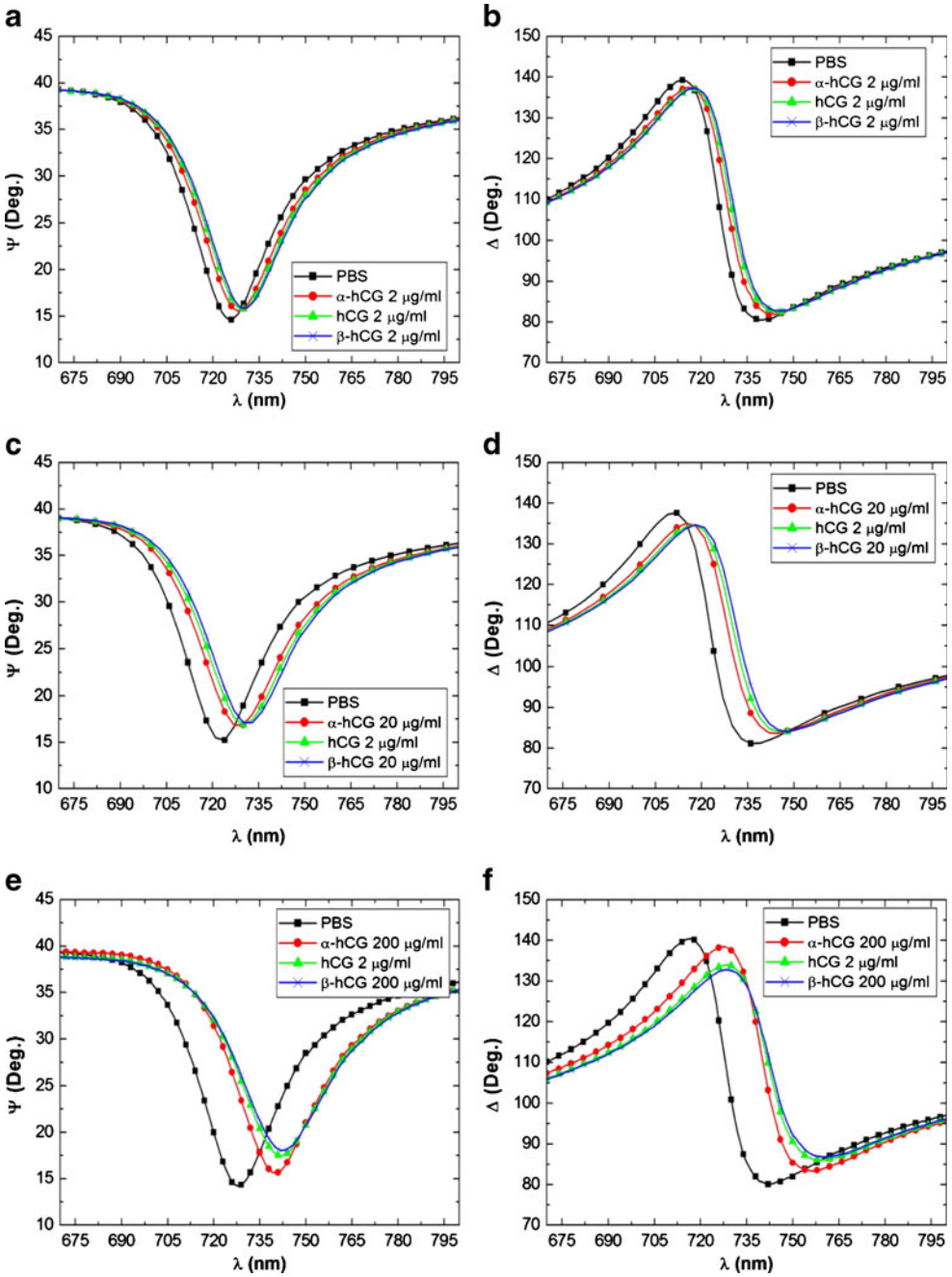

Fig. 8 Ψ and Δ spectral shifts for three hCG sandwich immunoassays after EDC/NHS activation: **a**, **b** anti-α-hCG and anti-β-hCG concentrations were 2 μg/ml, **c**, **d** anti-α-hCG and anti-β-hCG concentrations were 20 μg/ml, and **e**, **f** anti-α-hCG and anti-β-hCG concentrations were 200 μg/ml. The hCG concentration for the three assays was fixed at 2 μg/ml

The volume of each microwell was only 4.7 μl and the volume of analyte used for each reaction was 20–30 μl, which is a useful parameter when screening through a large number of variable parameters of bioassays. Binding of each layer of biomolecules caused a spectral shift for both Ψ and Δ spectra. Ellipsometric modelling and fitting allowed us to quantify the surface excesses of the bound biomolecules. The proposed TIRE technique could be a

Table 2 Fitting results and surface density calculation from the three assays in Fig. 8

Assay	Surface excess of anti-α-hCG (mg/m^2)	Surface excess of hCG (mg/m^2)	Surface excess of anti-β-hCG (mg/m^2)
Fig. 8a and b	0.91±0.04	0.39±0.02	0.23±0.01
Fig. 8c and d	1.87±0.03	0.60±0.02	0.41±0.07
Fig. 8e and f	4.37±0.12	0.84±0.09	0.28±0.06

hCG human chorionic gonadotrophin

very valuable tool for evaluating important parameters in immunoassays, DNA interactions, adsorption of biomolecules to solid surfaces or assessment of the reactivity of a functionalized polymer surface towards a specific analyte.

Acknowledgements This material is based upon work supported by the Science Foundation Ireland under grant no. 08/CE3/B754. D.E.W. is an E.T.S. Walton Visiting Fellow of Science Foundation Ireland. The authors would like to thank J. Garcia-Cordero for helping with the design and fabrication of the flow-cell. The authors also thank M. Stchakovsky and D. Sheppard from HORIBA Jobin Yvon for helping with the ellipsometric fitting.

References

1. Kameoko J, Craighead HG, Zhang H, Henion JA (2001) Anal Chem 73:1935–1941
2. Diaz-Quijada GA, Peytavi R, Nantel A, Roy E, Bergeron MG, Dumoulin MM, Veres T (2007) Lab Chip 7:856–862
3. Laib S, MacCraith BD (2007) Anal Chem 79:6264–6270
4. Pu Q, Oyesanya O, Thompson B, Liu S, Alvarez JC (2007) Langmuir 23:1577–1583
5. Jonsson C, Aronsson M, Rundstrom G, Pettersson C, Mendel-Hartvig I, Bakker J, Martinsson E, Liedberg B, MacCraith B, Ohman O, Melin J (2008) Lab Chip 8:1191–1197
6. Raj J, Herzog G, Manning M, Volcke C, MacCraith BD, Ballantyne S, Thompson M, Arrigan DWM (2009) Biosens Bioelectron 24:2654–2658
7. Volcke C, Gandhiraman RP, Gubala V, Raj J, Cummins T, Fonder G, Nooney RI, Mekhalif Z, Herzog G, Daniels S, Arrigan DWM, Cafolla AA, Williams DE (2010) Biosens Bioelectron 25:1875–1880
8. Gandhiraman RP, Volcke C, Gubala V, Doyle C, Basabe-Desmonts L, Dotzler C, Toney MF, Iacono M, Nooney RI, Daniels S, James B, Williams DE (2010) J Mater Chem 20:4116–4127
9. Gubala V, Gandhiraman RP, Volcke C, Doyle C, Coyle C, James B, Daniels S, Williams DE (2010) Analyst 135:1375–1381
10. Haake HM, Schutz A, Gauglitz G (2000) Fresenius J Anal Chem 366:576–585
11. Liedberg B, Nylander C, Lundström I (1995) Biosens Bioelectron 10:I–IX
12. Johansen K, Arwin H, Lundström I, Liedberg B (2000) Rev Sci Instrum 71:3530–3538
13. Green RJ, Davies J, Davies MC, Roberts CJ, Tendler SJB (1997) Biomaterials 18:405–413
14. Kugimiya A, Takeuchi T (2001) Biosens Bioelectron 16:1059–1062
15. Hook AL, Thissen H, Voelcker NH (2009) Langmuir 25:9173–9181
16. Westphal P, Bornmann A (2002) Sens Actuators B 84:278–282
17. Poksinski M, Arwin H (2003) Sens Actuators B 94:247–252
18. Arwin H, Poksinski M, Johansen K (2004) Appl Opt 43:3028–3036
19. Poksinski M, Arwin H (2004) Thin Solid Films 455–456C:716–721
20. Nabok A, Tsargorodskaya A, Hassan AK, Starodub NF (2005) Appl Surf Sci 246:381–386
21. Nabok A, Tsargorodskaya A, Davis F, Higson SPJ (2007) Biosens Bioelectron 23:377–383
22. Nabok A, Tsargorodskaya A, Holloway A, Starodub NF, Demchenko A (2007) Langmuir 23:8485–8490
23. Basova T, Plyashkevich V, Hassan A, Gürek AG, Gümüs G, Ahsen V (2009) Sens Actuators B 139:557–562
24. Balevicius Z, Vaicikauskas V, Babonas GJ (2009) Appl Surf Sci 256:640–644
25. Larsson A, Ekblad T, Andersson O, Liedberg B (2007) Biomacromolecules 8:287–295
26. Azzam RMA, Bashara NM (1992) Ellipsometry and polarized light. North Holland, Amsterdam
27. Le NCH, Yokokawa R, Dao DV, Nguyen TD, Wells JC, Sugiyama S (2009) Lab Chip 9:244–250
28. Palik ED (ed) (1985) Handbook of optical constants of solids. Academic, Orlando
29. Palik ED (ed) (1991) Handbook of optical constants of solids II. Academic, San Diego
30. Xu H, Lu JR, Williams DE (2006) J Phys Chem B 110:1907–1914
31. De Feitjer JA, Benjamins J, Veer FA (1978) Biopolymers 17:1759–1772
32. Liebermann T, Knoll W, Sluka P, Herrmann R (2000) Colloids Surf A 169:337–350
33. Larsson C, Rodahl M, Hook F (2003) Anal Chem 75:5080–5087
34. Xu H, Zhao X, Grant C, Lu JR, Williams DE, Penfold J (2006) Langmuir 22:6313–6320
35. Schult K, Katerkamp A, Trau D, Grawe F, Cammann K, Meusel M (1999) Anal Chem 71:5430–5435
36. Schneider BH, Dickinson EL, Vach MD, Hoijer JV, Howard LV (2000) Biosens Bioelectron 15:13–22
37. Boozer C, Yu Q, Chen S, Lee C, Homola J, Yee SS, Jiang S (2003) Sens Actuators B 90:22–30
38. Vareiro MMLM, Liu J, Knoll W, Zak K, Williams D, Toby A, Jenkins A (2005) Anal Chem 77:2426–2431